Optimizing postprocessing of range-gated viewing data for maritime search and rescue operations at night and bad weather conditions

Tristan Preis[1], Jendrik Schmidt[1], Alexander Klein[1], Enno Peters[1], Thomas Lübcke[2] and Maurice Stephan[1]

At night and bad weather conditions the detection of persons and objects floating in the sea represents a major challenge for search and rescue operations (SAR). If conventional searchlights are used, backscattering from rain, fog and snow decreases the detection range. Therefore, a compact and inexpensive range-gated viewing system was developed, which significantly reduces atmospheric backscattering. The instrument is designed for detection ranges of several hundred meters. In this study, different image processing techniques were analyzed in terms of improved object detectability for a human observer and for a machine learning based object detector, based on a real-world image dataset. On the one hand noise of the camera is reduced by performing a non-uniformity correction (NUC) and the other hand the dynamic range of the images is adjusted and dark objects are accentuated by equalizing (EQ). The aim of this field study with the subsequent post processing steps is to achieve with low computing power an improvement in visibility for both a human observer and a machine learning based object detector, which is based on a real-world image dataset. Results show, that processing requirements are different for both cases, mainly caused by the human eye perception, which an automated detector does not rely on and therefore the performance of the object detector before the equalizing step is slightly better. However, the NUC improves the image quality in any case.

KEY WORDS

~ vision enhancement
~ non-uniformity correction (NUC)
~ image processing
~ gated-viewing
~ range-gated viewing
~ equalization
~ object detection (YOLOv8)
~ maritime search and rescue operation (SAR)

[1]German Aerospace Center (DLR) Institute for the Protection of Maritime Infrastructures, Bremerhaven, Germany.
[2]German Maritime Search and Rescue Service (DGzRS), Bremen, Germany
e-mail: Tristan.Preis@dlr.de
doi: <this field will be filled by editorial board upon publishing of the article>
Received on: <date>; Revised on: <date>; Accepted on: <date>; Published online: <date>

1. INTRODUCTION

Even with a normal searchlight in the visible spectrum, objects with retroreflectors can be spotted at large distance and by far better than without reflectors. For this reason, many life vests and other objects designed to be seen, are equipped with retroreflectors (International Maritime Organization, 1989). However, in some cases, persons overboard do not wear special clothing with retroreflectors, which leads to a less bright reflection in the image and makes the detection more difficult, especially in harsh weather conditions. As a result, the main objective of this study, is to improve the visibility at night and scattering environments (fog, rain, snow) for operators at search and rescue operations (SAR) through optical instruments. In cooperation with the German Maritime Search and Rescue Service (Deutsche Gesellschaft zur Rettung Schiffbrüchiger, DGzRS) a field test comparing different camera technologies was performed at the German North Sea in the vicinity of Bremerhaven onboard the DGzRS rescue cruiser 'Hermann Rudolf Meyer' at December 6th, 2022 during nighttime (darkness).

As the available space and load is limited on a rescue cruiser, the size and weight of the system should be as small as possible. In addition, many rescue services depend on donations, which requires cost efficient solutions and instruments. Therefore, a Transportable RAnge-Gated VIewing System (TRAGVIS)[1] was developed, to detect persons overboard and other floating objects (Peters et al., 2019). In addition, the device should be simple to use and the images easy to interpret. For comparison, a thermal (IR) camera and a passive, monochrome visible-range (VIS) camera was used next to the range-gated viewing system.

Different scenes were recorded containing a dummy without retroreflectors and the rescue vessel's daughter boat. An example scene from the field test is shown in Figure 1. The figure shows identical scenes recorded simultaneously by the range-gated viewing system (Fig. 1a), the thermal camera (Fig. 1b) and the passive visible light camera (Fig. 1c), respectively. All images are raw data without any post-processing applied.

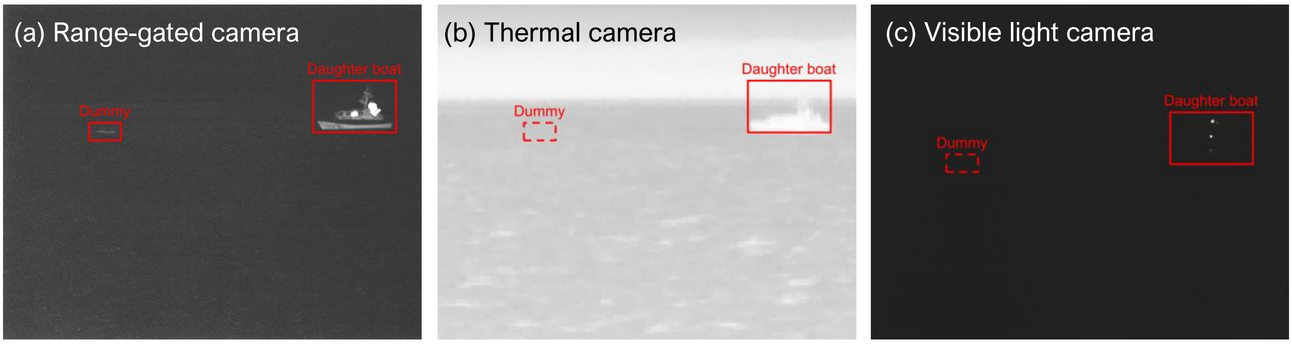

Figure 1. The same scene observed with (a) the range-gated viewing system, (b) thermal camera and (c) visible light camera. All images are raw data, i.e. without post-processing

The range gated image in Fig. 1a shows the rescue vessel's daughter boat and the dummy without retroreflectors. The major part of the image appears to be dark, as most of the light emitted is reflected from the water surface into the sky. In the thermal image (Fig. 1b), the daughter boat can be clearly identified, but the dummy is not distinguishable from the surrounding waves. While the thermal imaging camera is hardly affected by the backscatter, the image only shows the thermal distributions and not the objects, which is crucial when it comes to recognizing objects that have been floating in the sea for a longer time. In the visible image (Fig. 1c) taken without active illumination, everything is dark except for the navigational lights of the daughter boat. In comparison to the image recorded with TRAGVIS (Fig. 1a), the images shown in Figure 1b and Figure 1c provide no benefit for the search and rescue operator in terms of detecting the dummy (person overboard). However,

[1] In Section 2 the hardware of TRAGVIS is described more in detail.

even in the gated image, the dummy is hard to detect, especially when considering that search and rescue operations are often performed not in calm sea (as in this test) but in rough sea. This is why this study aims at improving TRAGVIS images further, enabling an even better (and more reliable) detection of persons and objects overboard spotted by human instrument operators and automated object detectors.

The study is structured as follows: The instrument and measurement technique of range-gated viewing is briefly explained in Section 2. Post-processing techniques improving the inspection of images are presented in Section 3, focusing on better recognition by human operators. In addition, an automatic, computer assisted object detector is introduced in Section 4 and was tested aiming to support the human search and rescue operator. For training of the algorithm, a labeled dataset from the field test is applied. After training, a selection of test images is used, to quantify the performance of the object detector. In Section 5, the results after the processing steps are evaluated and discussed with respect to the different object observer (human and automated detector). Section 6 provides a conclusion and outlook.

2. INSTRUMENT AND MEASUREMENT TECHNIQUE

The measuring setup and technique of range-gated viewing are shown in Figure 2. Fig. 2a provides a photo of the instrumental setup used on the rescue cruiser during the field test. The system consists of two housings: One for the visible (Onyx from Teledyne e2v) and thermal (VarioCAM HDx from InfraTec) camera, which are both passive cameras, and one for the range-gated viewing instrument, which consists of a special camera (Bora 2D from Teledyne e2v) equipped with a fast electronic shutter and a self-developed pulsed laser illuminator. The whole system is placed on a pan-tilt-unit (PTU) for sea stabilization and remote control.

The range-gating (also known as gated-viewing) technology attempts to physically reduce backscattering from rain, fog or snow in front of the sensor system (Laurenzis, 2012). The measuring technique is to illuminate and record a specific depth level of a scene, as illustrated in Fig. 2b. A pulsed laser illuminator is synchronized with a camera, that can open and close its electronic shutter typically within nanoseconds. The adjustable delay between emission of the laser pulse and opening of the camera shutter allows to exclude non-essential parts of an image, which then consists of a defined gate, that is exposed.

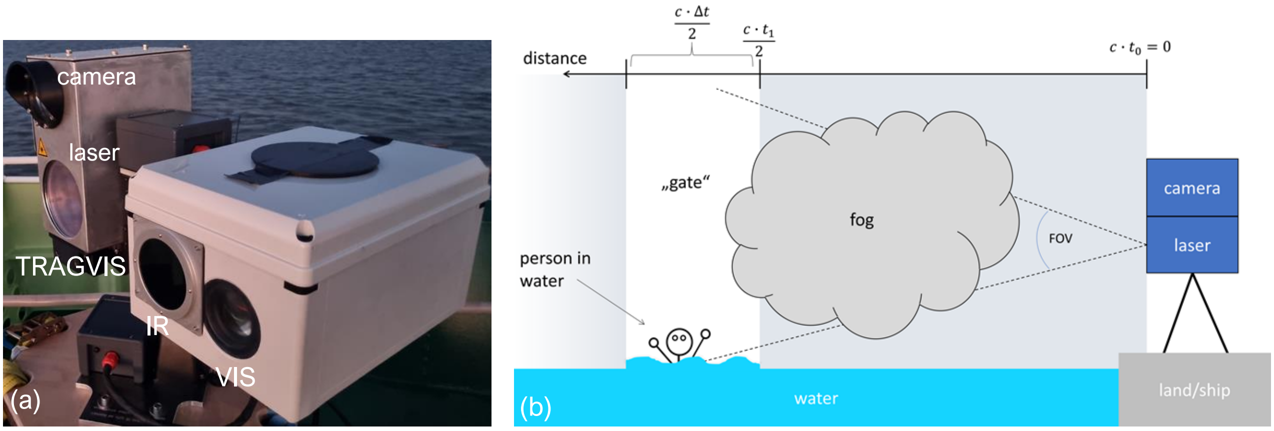

Figure 2 (a) Measuring setup at rescue cruiser with range-gated viewing system consisting of camera (top) and laser illuminator (bottom) (TRAGVIS), thermal and VIS camera; (b) Measuring technique of range-gated viewing.

After emission of a laser pulse at time t_0, the camera shutter stays closed, while the pulse propagates towards the gate. Due to the closed shutter, backscattering from particles along the light path is not recorded by the camera, i.e. the region between the instrument and the gate stays dark in the recorded image. At time t_1 the camera shutter opens and the first reflections of the pulse are recorded. When the camera and laser are at the same location, the distance of the rising edge of the gate d_{gf} is half of time t_1 multiplied with the speed of light c:

$$d_{gf} = c \cdot t_1/2 \qquad (1)$$

Similarly, the gate width Δt is defined by the width of the laser pulse and open camera shutter. This process is repeated ca. 17000 times (taking about 50 ms) to accumulate enough photons before the camera is finally read out (which again takes some milliseconds). The effective framerate the instrument provides is therefore 16-17 images/sec.

Many range-gated viewing systems operate in the short-wavelength infrared (SWIR) spectrum at 1.57 µm and new approaches tend to use the 2.09 µm spectrum (Göhler et al., 2023). The advantage of these spectra is the reduction of atmospheric scintillation, however, this is associated with high costs, as the sensors are made of indium gallium arsenide (InGaAs) or mercury cadmium telluride (MCT). TRAGVIS operates at approximately 808 nm and is equipped with a CMOS camera, which has a sensor with a good quantum efficiency of 42 % in the near-infrared (NIR) spectrum. This design decision was made to reduce construction costs and because Mie calculations have shown that longer wavelengths (SWIR) have no advantage in terms of scattering and extinction efficiencies when fog particles consisting of water are large (Peters et al., 2023), which is typically the case in the environments TRAGVIS was designed for. Interestingly, Bett et al. (2023) proposed using a single-pixel camera, which is another attempt potentially reducing costs. However, the image must be then generated with the help of a neural network, which requires computing power and training datasets, and thus a traditional approach was used here.

As the main objective of TRAGVIS is to find people in distress at sea, a wide field of view (FOV) of 7° x 6° was chosen (which roughly matches the FOV of standard binoculars) to cover a large area in each image. The maximum detection range under fog conditions is approximately 250 m. To address eye-safety as a major concern, a self-build beam expander was developed. The resulting instrument fulfills the requirement of a laser class 1M system.[2]

Previous measurements have shown, that for moderate aerosol loads as prevailing during the field test reported here, the first 50 m contribute the most backscattering to an image. Consequently, the recorded images in this paper suppress the first 50 m only, which is sufficient for an improved image and also enables a wide gate. The reason of this is the speed of recording a full scene. Normally a range-gating instrument provides a sequence of images, in which the position of the gate varies and images then need to be combined. This also enables obtaining depth information, but for the purpose of this study depth information is not needed.

3. POST-PROCESSING

Gated-viewing images usually suffer from large fixed pattern noise decreasing the image quality. After acquiring an image, a non-uniformity correction (NUC) is performed. A corrected 1-point NUC $\boldsymbol{x}_{1-NUC}$ image is calculated by subtracting a reference dark image $\boldsymbol{x}_{ref,dark}$ from the recorded image $\boldsymbol{x}_{obj}$, which corrects for the so-called dark signal non-uniformity (DSNU):

$$\boldsymbol{x}_{1-NUC} = \boldsymbol{x}_{obj} - \boldsymbol{x}_{ref,dark} \qquad (2)$$

The dark image is acquired with a mechanically closed instrument preventing any light from reaching the sensor. In addition, the dark image is the average over 100 single exposures to average out temporal noise, so that the final dark image consists of spatial patterns only.

[2] Further technical information can be found in Peters et al., 2019

After the subtraction of the dark image, the mean gray value $\overline{x_{ref,dark}}$ can be added to all pixels resulting in an image $\boldsymbol{x}_{1-NUC,mean}$ having the same background gray value:

$$\boldsymbol{x}_{1-NUC,mean} = \boldsymbol{x}_{obj} - \boldsymbol{x}_{ref,dark} + \overline{x_{ref,dark}} \quad (3)$$

The idea of a further 2-point NUC is to reduce the spatial noise, caused by the different sensitivities of the pixels when exposed to light, which leads to the so-called Photo-Response Non-Uniformity (PRNU). Therefore, matrix $\boldsymbol{m}$ is introduced. The matrix is obtained from a reference image $\boldsymbol{x}_{ref,mid}$, in which the sensor is illuminated by a homogenous light (usually at approx. 50% saturation), and a reference dark image $\boldsymbol{x}_{ref,dark}$:

$$\boldsymbol{m} = \left(\overline{x_{ref,mid}} - \overline{x_{ref,dark}}\right) / \left(\boldsymbol{x}_{ref,mid} - \boldsymbol{x}_{ref,dark}\right) \quad (4)$$

After multiplying an uncorrected raw image, from which the dark image has been subtracted, with $\boldsymbol{m}$, all pixel photo responsivities have the same slope[3]. As for the 1-point NUC, the mean gray value of the dark image might ($\boldsymbol{x}_{2-NUC,mean}$) or might not ($\boldsymbol{x}_{2-NUC}$) be added to the corrected image:

$$\boldsymbol{x}_{2-NUC,mean} = \left(\boldsymbol{x}_{obj} - \boldsymbol{x}_{ref,dark}\right)\boldsymbol{m} + \overline{x_{ref,dark}} \quad (5)$$

$$\boldsymbol{x}_{2-NUC} = \left(\boldsymbol{x}_{obj} - \boldsymbol{x}_{ref,dark}\right)\boldsymbol{m} \quad (6)$$

To highlight more details, the image can be equalized (EQ). Most parts in images recorded during night over water are usually dark. Simply brightening the scene results in a milky appearance with no benefit for the human operator, thus a more sophisticated solution is required. In addition, the instrument provides 12 bit raw data while displays work on 8 bit, thus a conversion from 12 bit to 8 bit is required. As diffuse reflections from distant objects are usually very small, low signals should be brightened up more than large signals in order to increase perception by human operators. Therefore, an equalizer algorithm is adopted, that is usually used for astrophotography[4]. The equalization process can be separated into two functions $f(x)$ and $g(x)$, which are called one after the other.

The function $f(x)$ is boosting dark gray values towards brighter values, as shown in Figure 3. Details at the dark gray scale are more contrasted. Function $g(x)$ pushes dark and bright pixel values to the middle of the gray value range.

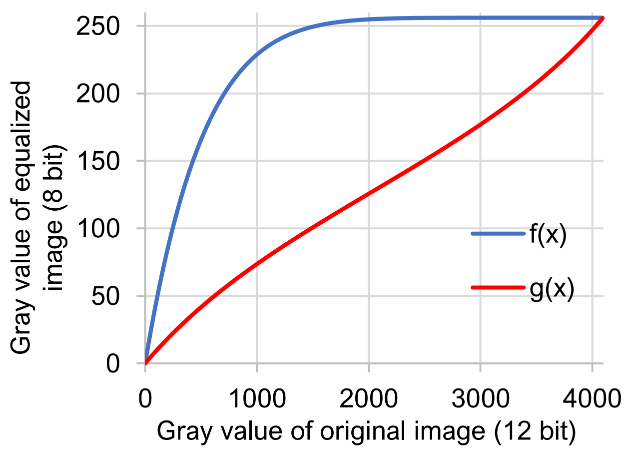

Figure 3. Equalization graphs including 12 bit to 8 bit conversion.

---

[3] The 2-point NUC suggested here assumes a linear photo-response.
[4] https://yager.io/Astro.html#Post-processing, 22.02.2024

Table 1 summarizes all combinations of corrections and equalizations performed during post-processing. To identify the optimal method, all processing combinations were performed for each image recorded by TRAGVIS. Resulting in ten different images of the same scene, which are then compared with each other.

Processing configuration
Original – raw TRAGVIS image
1-point NUC
2-point NUC
1-point NUC + mean
2-point NUC + mean
Original + EQ
1-point NUC + EQ
2-point NUC + EQ
1-point NUC + mean + EQ
2-point NUC + mean + EQ

Table 1. List of processing steps and resulting images.

4. AUTOMATED OBJECT DETECTION

Besides manual detection by human observers, automated, machine learning-based object detectors can assist the SAR forces. The image processing requirements for automated detectors may vary from what a human observer defines as good image quality. Therefore, the same set of images with processing configurations has been tested using a machine learning based object detector.

A large number of different algorithms for object detection is available nowadays. Models such as Region-based Convolutional Neural Networks (R-CNN) (Girshick, Ross, et al., 2014) use a two-stage process, where in the first place general object areas are proposed and then in a second set, the object is classified and the localization is refined further. Currently, detection transformer models produce the best results (Carion et al., 2020). Given the need to apply the detector in real time on limited hardware, SAR purposes require the detector to be as fast as possible, while delivering accurate results. As a detailed evaluation on the recorded, relatively small dataset is not meaningful between different object detectors, this work focuses on the use of the newest version of the object detector YOLO, specifically YOLOv8 (Ultralytics, 2023) for automatic detection tasks, which is a widely used and well-known algorithm. YOLO uses only a single end-to-end pipeline to acquire the object class and bounding box, which makes it one of the fastest modern object detectors.

This work compares models YOLOv8n with 3.2 million and YOLOv8x with 68.2 million parameters. Both models were pretrained on the COCO dataset, which is integrated in the YOLO algorithm. Pretraining is used to set the object detector in advance so that it can then recognize edges and other geometric structures. It is not the task of the pretraining to detect ships and other maritime objects, so it does not matter whether the object detector analyzes images at night or during the day. After pretraining, the training dataset is used to fully train the object detector for 100 epochs using the full image size of 1280 x 1024 pixels. For training and evaluation, the dataset was split in 461 training and 38 test images. The training and test datasets were also expanded with each processing step (s. Tab. 1), so that in the end 4610 images for training and 380 images for evaluation are available. All the training data was learned together in the object detector. The test set is split up for each processing configuration given in Table 1, to compare the influence on the detection quality.

5. RESULTS

As mentioned in Section 4, during the field test 499 different scenes were recorded with TRAGVIS. The scene already shown in Fig. 1 is used to demonstrate the effect of the processing techniques described in Section 3. Fig. 4 summarizes different combinations using a 1-point NUC. Because of the subtraction of the reference dark image $\boldsymbol{x}_{ref,dark}$, the resulting image in Fig. 4a for the 1-point NUC is generally darker. For human observers, the recognition of the dummy in contrast to the background gets worse, as the human eye distinguishes contrasts between dark gray levels worse compared to bright gray levels on most computer displays and monitors (Kimpe and Tuytschaever, 2007). Therefore, the dummy can be better identified, when adding the mean gray value of the reference dark image as in Fig. 4b. The results after equalization are shown in Fig. 4c and Fig. 4d. A significant improvement can be observed in the image with 1-point NUC and equalization without addition of the average (Fig. 4d), the dummy can be spotted better in comparison to the other processing configurations.

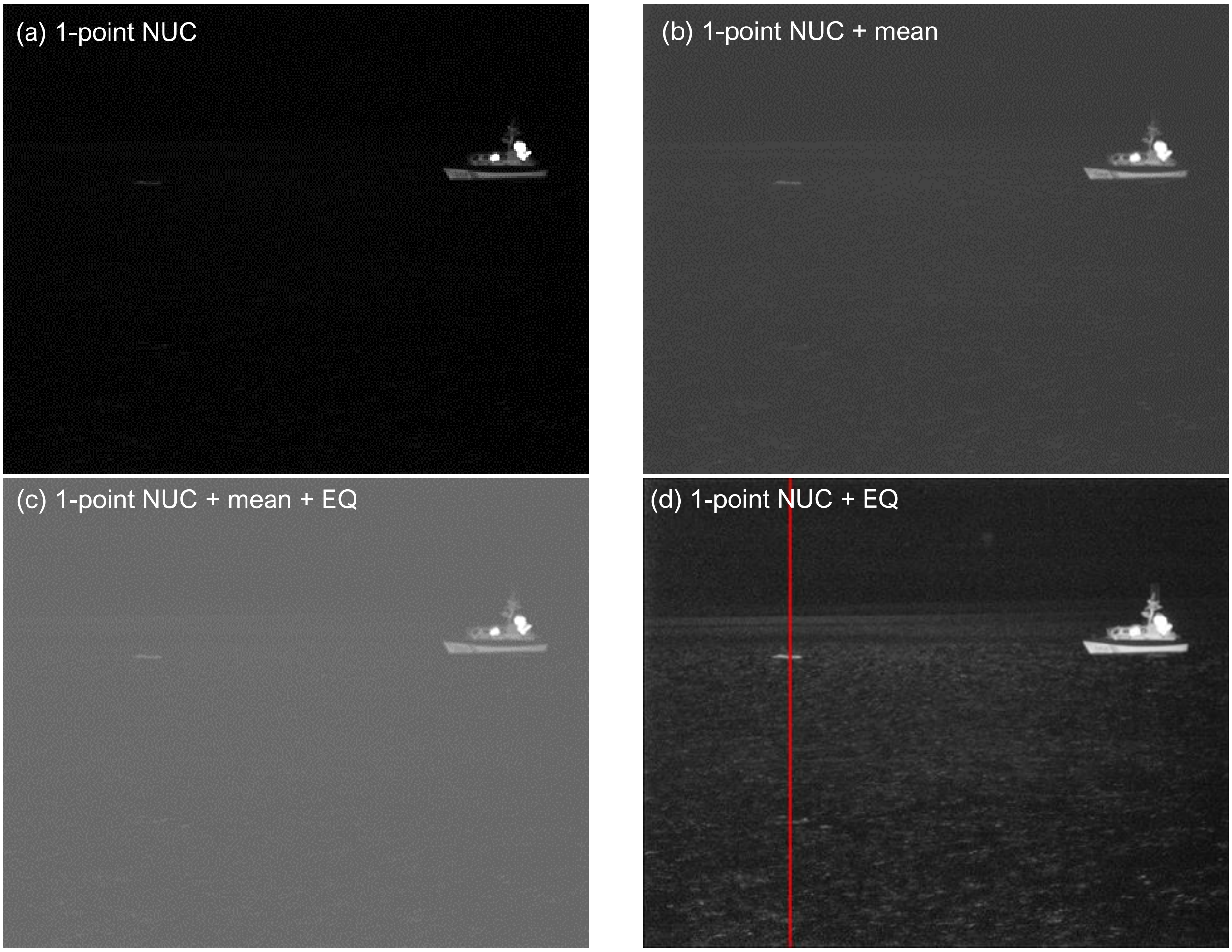

Figure 4. Range-gated images with different preprocessing configurations: (a) 1-point NUC, (b) 1-point NUC with added mean gray value (c) 1-point NUC with added mean gray value after equalization and (d) 1-point NUC after equalization with vertical cross section to get the contrast between dummy and background (s. Fig. 5).

To quantify the effect of different preprocessing configurations on the detection of the dummy, the gray values along a vertical line through the position of the dummy were analyzed. In Figure 5 the cross section along the indicated line in Fig. 4d is shown. The dummy is pointing out with a gray value of 148 in comparison the average of 42 along the indicated line. Based on the excess of the dummy over the background gray value, the

Michelson contrast (C_M) (Michelson, 1927) was calculated. The Michelson contrast was calculated between dummy (x_{max}) and average of the background (x_{med}):

$$C_M = (x_{max} - x_{med})/(x_{max} + x_{med}) \dots\dots (6)$$

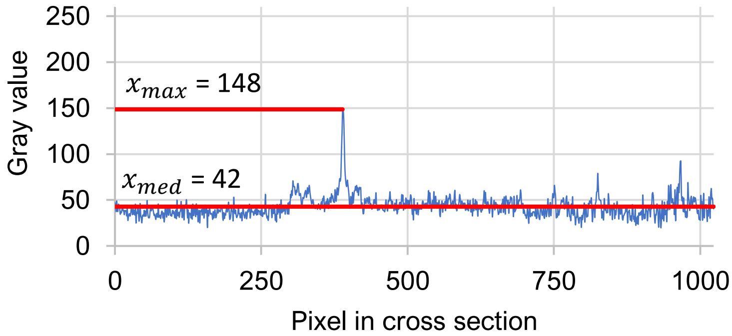

Figure 5. Gray values along the red line in Fig. 4d.

The contrast of the original image and the images after the non-uniformity correction with the added mean value is similar. Not adding the mean gray value in the NUC increases the contrast significantly. However, this has to be taken with care because, as mentioned before, the human eye perceives differences better between bright gray levels on computer displays. That can be seen from Fig. 4a (1-point NUC) and b (1-point NUC + mean): For the human observer, the dummy is almost invisible in Fig. 4a, while it is much better seen, when adding the background mean in Fig. 4b. However, the calculated Michelson contrast in Table 2 is 0.86 for Fig. 4a and is as small as the original image with 0.23 for the configuration shown in Fig 4b. The reason is in the definition of the Michelson contrast (eq. 6). The smaller the background gray value is, the closer to 1 the contrast will get. To conclude, the Michelson contrast is not a good measure for the benefit of the postprocessing in case of a human observer.

Processing step	Michelson contrast	Precision	Recall
Original	0.22	0.94	0.83
1-point NUC	0.86	0.96	0.83
2-point NUC	0.85	0.96	0.86
1-point NUC + mean	0.23	0.96	0.82
2-point NUC + mean	0.22	0.96	0.83
Original + EQ	0.13	1.00	0.75
1-point NUC + EQ	0.71	0.95	0.76
2-point NUC + EQ	0.71	0.93	0.85
1-point NUC + mean + EQ	0.12	0.92	0.83
2-point NUC + mean + EQ	0.12	0.88	0.90

Table 2. Michelson contrast for every processing step and object detection results (precision and recall) of test images for YOLOv8n for class ‘Fixed and Floating Objects’ (i.a. dummy)

The 2-point NUC increases the image quality usually more than the 1-point NUC. In this investigation, however the 2-point NUC leads to very similar results than the 1-point NUC. The reason is, that the images are mostly dark, the influence of the pixel sensitivity can be neglected, compared to the influence of the dark signal non-uniformity. In difference to a human observer, a machine learning based detector, performs best for a different configuration of postprocessing steps.

In Table 2 also the precision and recall for the dummy is summarized when using the object detector. Precision is defined as correct detected objects divided by the total number of detections by the object detector (including false detections). In contrast, the definition of recall is the proportion of correct detected objects to all objects of relevance. Objects of relevance are the number of labeled objects in the test dataset.

By comparing the results of the object detector with the Michelson contrast in Table 2, the object detector tends to perform better, when the Michelson contrast is large. The reason is most likely that edges are detected better. The best results are obtained for the 1-point NUC and 2-point NUC before equalization, which have the highest contrast. All other processing variants are tradeoffs between precision and recall, compared to the original raw image.

6. CONCLUSION

The used low-cost and lightweight range-gated viewing system represents an advantage in finding persons in distress and other floating objects in the sea over thermal imaging and visible light records. In this study, non-uniformity correction and the equalizer algorithm were used, two image post-processing technologies that require low computing power and can therefore also be run on small computing units. Range-gated viewing (on the hardware side) and non-uniformity correction and equalization (on the software side) improve the object detection for a human search and rescue operator and an automated object detector. Nevertheless, different postprocessing configurations were found to give best results.

In the case of a human operator, 1-point NUC and 2-point NUC after equalization is the best option, because shifting the dark dummy to the middle of the grayscale supports human perception. In addition, the Michelson contrast was found to be not a good measure for identifying the optimal postprocessing configuration for human perception, which is specific to the case having dark background and dark objects of interest. In contrast, for automated object detection, mean gray level of the image does not play a role in detection capability. Processing steps, which produce images with the highest contrast, deliver the best results for automated object detection. In this case the 1-point NUC and 2-point NUC before equalization deliver the best results, because the equalization, although helping the human perception, decreases the Michelson contrast.

For both object detection methods, the 2-point NUC provides no significant benefit to the 1-point NUC (because the image is mainly dark and thus suffering predominantly from DSNU), but is more complex and consumes computational power, so the recommendation is to perform the 1-point NUC only, especially when it comes to saving space and computing power so that the system can also be used on a rescue vessel.

As an outlook, for future investigations other equalizer algorithms should be investigated. Besides the introduced techniques, other mechanisms, like filtering and masking for vision enhancement should be evaluated.

7. ACKNOWLEDGMENTS

We acknowledge the crew of the search and rescue vessel ‘Hermann Rudolf Meyer’ from the German Maritime Search and Rescue Service (DGzRS) supporting the field test. The technical and scientific work presented here, was funded by the Federal Ministry for Economic Affairs and Climate Action of Germany (Bundesministerium für Wirtschaft und Klimaschutz, BMWK) and the state of Bremen.

REFERENCES

Bett, C., Daiber-Huppert, M., Frenner, K., Osten, W. (2023). Evaluation of a time-gated-single-pixel-camera as a promising sensor for autonomous vehicles in harsh weather conditions. In: J. Eur. Opt. Society-Rapid Publ. 19 (1), S. 27. DOI: 10.1051/jeos/2023023.

Carion, N., Massa, F., Synnaeve, G., Usunier, N., Kirillov, A., & Zagoruyko, S. (2020, August). End-to-end object detection with transformers. In European conference on computer vision (pp. 213-229). Cham: Springer International Publishing.

Girshick, R., Donahue, J., Darrell, T., & Malik, J. (2014). Rich feature hierarchies for accurate object detection and semantic segmentation. In Proceedings of the IEEE conference on computer vision and pattern recognition (pp. 580-587).

Göhler, B., Lutzmann, P., Walter, D., Bürsing, H., Deutsch, J., Eichhorn, M., Kieleck, C., Sieck, A., Wiegleb, R. (2023 October). Gated viewing at 2.09 µm laser wavelength: experimental system assessment and comparison to 1.57 µm, Proc. SPIE 12737, Electro-Optical and Infrared Systems: Technology and Applications XX, 127370C; https://doi.org/10.1117/12.2684727

International Maritime Organization (1989) RESOLUTION A.658(16) - Use and Fitting of Retro-Reflective Materials on Life-Saving Appliances. https://wwwcdn.imo.org/localresources/en/KnowledgeCentre/IndexofIMOResolutions/AssemblyDocuments/A.658(16).pdf

Kimpe, T., Tuytschaever, T. (2007). Increasing the number of gray shades in medical display systems–how much is enough? J Digit Imaging. 2007 Dec;20(4):422-32. doi: 10.1007/s10278-006-1052-3. PMID: 17195900; PMCID: PMC3043920.

Laurenzis, M. (2012). Investigation of range-gated imaging in scattering environments. Optical Engineering. 51. 061303. 10.1117/1.OE.51.6.061303.5

Michelson A. A. (1927). Studies in optics. University of Chicago Press.

Peli E. (1990). Contrast in complex images. J Opt Soc Am A. 1990 Oct;7(10):2032-40. doi: 10.1364/josaa.7.002032. PMID: 2231113.

Perry, D. & Dereniak, E. (1993). Linear theory of nonuniformity correction in infrared staring sensors. Optical Engineering. 32. 1854-1859. 10.1117/12.145601

Peters, E., Anders, M. , Preis, T. , Kontschak, L., Schmidt, J., Stephan, M. (2023). Performance studies of two active SWIR instrument designs for vision enhancement in indoor applications, Proc. SPIE 12737, Electro-Optical and Infrared Systems: Technology and Applications XX, 127370Z (23 October 2023); https://doi.org/10.1117/12.2680281

Peters, E., Schmidt, J., Juranyi, Z., Berger, M., Scherbarth, S., Lehmann, F. (2019). Development of a novel low-cost NIR gated-viewing sensor for maritime search and rescue applications. 3. 10.1117/12.2532538.

Ultralytics. (2023). https://docs.ultralytics.com/, 22.02.2024